Interaction of a shear Alfvén wave with a filamentary density perturbation in a low-β plasma

T. Drozdenko[a] and G. J. Morales
Department of Physics and Astronomy, University of California at Los Angeles, Los Angeles, California 90095

(Received 8 October 1999; accepted 2 December 1999)

This analytic study investigates the interaction between a large-scale shear Alfvén wave propagating through a low-β plasma and a pre-existing density perturbation of small transverse scale. The interaction forms an *in situ* antenna that self-consistently generates two field-aligned current channels of opposite polarity. The expansion of the current channels across the confining field is bounded by the cone trajectories of small-scale inertial Alfvén waves. The spatial patterns of the radiated fields are obtained, and the magnitude of the parallel electric field and its effective phase velocity are assessed. An effective cross section that varies with the parallel and transverse scale lengths of the density perturbation summarizes the efficiency of the direct conversion process. © *2000 American Institute of Physics.* [S1070-664X(00)02703-8]

I. INTRODUCTION

Presently, there is significant interest in understanding how the large energy content of a long wavelength Alfvén wave can be transferred to ambient plasma particles. This topic impacts several areas of contemporary plasma research including magnetic reconnection studies,[1] formation of auroral beams,[2] solar corona heating,[3] and energy transport[4] in magnetic confinement devices. It is widely recognized that in order for an effective wave–particle interaction to occur, the scale of the primary wave transverse to the confining magnetic field must be contracted to a length comparable to the electron skin-depth or the ion gyroradius. In such circumstances, significant parallel electric fields can develop and transit–time interactions due to the field gradients can affect both ions and electrons.

The present analytic study focuses on a specific process that can naturally give rise to such a transformation of spatial scales. The process is expected to play an important role in nonequilibrium situations where large levels of density fluctuations are found. Specifically, this analytic study examines the direct conversion of a plane, shear Alfvén wave initially propagating along the magnetic field direction (i.e., with $k_\perp = 0$) into narrow, collimated shear modes due to the interaction with a pre-existing density filament in the ambient plasma. Analogous transformations have been studied analytically[5] for compressional Alfvén waves above the cyclotron frequency in the context of wave-heating of tokamak plasmas. The direct conversion process has been observed in the laboratory,[6] in space[7] for whistler modes and in ionosperic experiments[8] involving Langmuir waves.

The manuscript is organized as follows. The mathematical formulation of the problem is presented in Sec. II where expressions for the small-scale electric and magnetic fields are given in terms of integrals that can be readily evaluated numerically. The detailed properties obtained from the numerical evaluation of the intregrals are discussed in Sec. III and compared to various analytic limits. An ''effective cross section'' for the process is considered in Sec. IV. Conclusions are presented in Sec. V.

II. FORMULATION

This study considers the localized excitation of a small-scale shear Alfvén wave in a cold magnetized plasma. The analysis applies to the ''inertial regime'' in which $\beta_e \ll m/M$, where $\beta_e = 4\pi n T_e / B_0^2$, n is the plasma density, T_e is the electron temperature, B_0 is the strength of the confining magnetic field, and m and M are the electron and ion mass respectively. A Cartesian coordinate system (x,y,z) is used in which the confining magnetic field points along the z direction.

A primary (or pump) shear Alfvén wave is assumed to be excited remotely and propagates along the positive z direction with negligible transverse wave number $(k_\perp = 0)$. The ambient plasma is uniform except for a filamentary density perturbation located at the origin of the coordinate system. The density filament is described by

$$\delta\tilde{n}(x,y,z) = \delta n \exp\left(-\frac{\rho^2}{2L_\perp^2} - \frac{z^2}{2L_\parallel^2} \right), \tag{1}$$

where $\rho^2 = x^2 + y^2$ and $L_\perp$ and $L_\parallel$ are the transverse and axial scales of the perturbation. In this formulation, we consider $L_\perp$ and $L_\parallel$ to be much smaller than the wavelength of the primary wave. A schematic of the geometry of the problem is given in Fig. 1.

The electric and magnetic fields of the pump wave of frequency ω are given by

$$\mathbf{E}_p = E_p e^{i(k_A z - \omega t)} \hat{\mathbf{x}} + \text{c.c.}, \tag{2}$$

$$\mathbf{B}_p = B_p e^{i(k_A z - \omega t)} \hat{\mathbf{y}} + \text{c.c.}, \tag{3}$$

where $k_A = \omega / v_A$ and $v_A = B_0 / \sqrt{4\pi M n}$ is the Alfvén speed of the uniform plasma.

[a]Electronic mail: tara@physics.ucla.edu

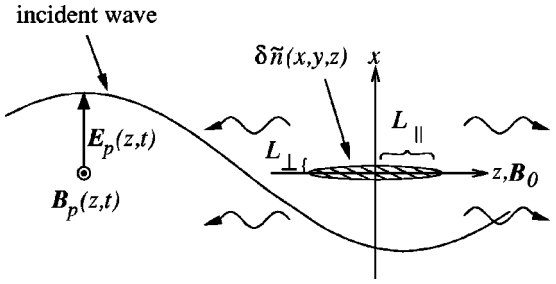

FIG. 1. Schematic of the problem considered. A large scale Alfvén wave of frequency ω (with $k_\perp = 0$) is incident on a field-aligned density perturbation having axial and transverse scale lengths $L_\parallel$ and $L_\perp$, with $L_\parallel \gg L_\perp$ and $L_\perp$ on the order of the electron skin-depth. The interaction gives rise to right and left-going collimated shear waves having finite parallel electric fields.

We envision the magnitude of the density perturbation to be sufficiently small so that there is no need to consider the modification that it causes on the structure of the pump wave. In separate numerical studies we have found this approximation to be quite good even for relatively large values of $|\delta n|$. This occurs because shear waves do not exhibit a cutoff or a resonance as the density is varied locally.

In the low-frequency regime $\omega \ll \Omega_i$, where Ω_i is the ion cyclotron frequency, the cold ions having charge q experience an oscillatory polarization velocity due to the pump wave,

$$\mathbf{v}_p = \frac{-q\omega}{M\Omega_i^2}(iE_p e^{i(k_A z-\omega t)}\hat{\mathbf{x}} + \text{c.c.}). \tag{4}$$

This velocity beats with the density perturbation generating a source current,

$$\mathbf{j}_s = q\,\delta\tilde{n}\mathbf{v}_p, \tag{5}$$

which acts as an *in situ* antenna. It should be noted that this antenna is linearly polarized along the x direction and constitutes a clear example of a pure transverse exciter. In constrast, the disk exciters previously used in the laboratory[9,10] to generate shear Alfvén waves of small transverse scale[11,12] couple to the shear wave through the modulation of axial currents carried by electrons.

The field components F_j that arise in the calculation have space–time dependence of the form

$$F_j(\mathbf{r},t) = \int_{-\infty}^{+\infty}\frac{dk_z}{(2\pi)}\int_0^{+\infty}\frac{dk_\perp k_\perp}{(2\pi)}\int_0^{2\pi}\frac{d\alpha}{(2\pi)} \times e^{i(\mathbf{k}\cdot\mathbf{r}-\omega t)}\tilde{F}_j(\mathbf{k},\omega) + \text{c.c.}, \tag{6}$$

where α is the azimuthal angle in a cylindrical coordinate system in k-space. The transform of the source current takes the form

$$\tilde{J}_s(\mathbf{k},\omega) = -i(2\pi L_\perp^2)\sqrt{2\pi L_\parallel}\left(\frac{\delta n}{n_0}\right)\frac{n_0 q^2\omega E_p}{M\Omega_i^2} \times e^{-L_\perp^2 k_\perp^2/2} e^{-L_\parallel^2(k_z-k_A)^2/2}\hat{\mathbf{x}}, \tag{7}$$

and appears in the Fourier-transformed wave equation

$$\mathbf{k}\times\mathbf{k}\times\tilde{\mathbf{E}} + k_0^2\overleftrightarrow{\epsilon}\cdot\tilde{\mathbf{E}} = -i\left(\frac{4\pi k_0}{c}\right)\tilde{J}_s, \tag{8}$$

where $k_0 = \omega/c$, with c the speed of light. $\overleftrightarrow{\epsilon}$ is the dielectric tensor appropriate for the description of the linear response of a cold plasma to a low-frequency Alfvén wave

$$\overleftrightarrow{\epsilon}(\omega) = \begin{pmatrix} \epsilon_\perp & 0 & 0 \\ 0 & \epsilon_\perp & 0 \\ 0 & 0 & \epsilon_\parallel \end{pmatrix}, \tag{9}$$

with $\epsilon_\perp \approx (c/v_A)^2$ and $\epsilon_\parallel \approx -(\omega_{pe}/\omega)^2$, where ω_{pe} is the electron plasma frequency.

Using Eq. (8) to solve for the electric field components yields

$$\tilde{E}_x = \frac{\tilde{\mathcal{J}}_{sx}}{k_0^2\epsilon_\parallel D(\mathbf{k},\omega)}[(k^2-k_0^2\epsilon_\perp)(k^2-k_0^2\epsilon_\parallel) - k_\perp^2\sin^2\alpha(k^2-k_0^2\epsilon_\parallel) - k_z^2(k^2-k_0^2\epsilon_\perp)], \tag{10}$$

$$\tilde{E}_y = \frac{\tilde{\mathcal{J}}_{sx}}{k_0^2\epsilon_\parallel D(\mathbf{k},\omega)}[k_\perp^2\sin\alpha\cos\alpha(k^2-k_0^2\epsilon_\parallel)], \tag{11}$$

$$\tilde{E}_z = \frac{\tilde{\mathcal{J}}_{sx}}{k_0^2\epsilon_\parallel D(\mathbf{k},\omega)}[k_z k_\perp\cos\alpha(k^2-k_0^2\epsilon_\perp)], \tag{12}$$

where $\tilde{\mathcal{J}}_{sx} = -i(4\pi k_0/c)\tilde{J}_s\cdot\hat{\mathbf{x}}$, and $D(\mathbf{k},\omega)$ is given by

$$D(\mathbf{k},\omega) = (k_z^2-k_1^2)(k_z^2-k_2^2),$$

with

$$k_1^2 \equiv k_0^2\epsilon_\perp - k_\perp^2\epsilon_\perp/\epsilon_\parallel,$$

and

$$k_2^2 \equiv k_0^2\epsilon_\perp - k_\perp^2.$$

Using Faraday's Law to obtain the self-consistent magnetic-field components excited by the beat antenna results in

$$\tilde{B}_x = -k_0 k_z\frac{\tilde{\mathcal{J}}_{sx}}{k_0^2\epsilon_\parallel D(\mathbf{k},\omega)}[k_\perp^2\sin\alpha\cos\alpha(\epsilon_\perp-\epsilon_\parallel)], \tag{13}$$

$$\tilde{B}_y = -k_0 k_z\frac{\tilde{\mathcal{J}}_{sx}}{k_0^2\epsilon_\parallel D(\mathbf{k},\omega)}[k_\perp^2\epsilon_\perp\sin^2\alpha - k_0^2\epsilon_\perp\epsilon_\parallel + (k_\perp^2\cos^2\alpha + k_z^2)\epsilon_\parallel], \tag{14}$$

$$\tilde{B}_z = -k_0 k_y\frac{\tilde{\mathcal{J}}_{sx}}{k_0^2\epsilon_\parallel D(\mathbf{k},\omega)}[k_0^2\epsilon_\perp\epsilon_\parallel - k_z^2\epsilon_\parallel - k_\perp^2\epsilon_\perp]. \tag{15}$$

The zeros of $D(\mathbf{k},\omega)$ lead to dispersion relations for two different types of Alfvén waves. The shear polarization corresponds to $k_z = k_1$, and the compressional mode corresponds to $k_z = k_2$. For the narrow transverse scales associated with the filamentary perturbations of interest to this study, we have found that the fields of the compressional mode excited by the beat antenna are at least three orders of magnitude smaller than those of the shear mode. Hence, in

the remaining calculation presented here, we neglect the contribution of the compressional mode and make the approximation

$$\frac{1}{D(\mathbf{k},\omega)} \rightarrow \frac{1}{(k_1^2-k_2^2)}\left(\frac{1}{k_z^2-k_1^2}\right). \tag{16}$$

Since we are interested in determining the spatial structure of the fields radiated by the beat antenna, the inverse transform of each component must be performed, i.e., Eq. (6) must be evaluated for each field component. Note that it is useful to represent the fields in terms of cylindrical coordinates (ρ,z,ϕ). The angular dependence on ϕ is necessary because the beat antenna is dipole-like (oriented along the x direction) and thus radiates modes that are not azimuthally symmetric. Again, this analysis differs from the analysis of symmetric disk exciters used in laboratory studies.[11,12]

It is possible to perform the integrations over α and k_z analytically for all the field components. However, the integration over $k_\perp$ is not tractable and must be evaluated numerically. To properly parametrize the dependencies of these integrals it is useful to introduce the scaled variables $\kappa = k_\perp/k_s$, $\overline{\rho}=k_s\rho$, $l_\perp = k_s L_\perp$, $l_\parallel = k_A L_\parallel$, $\xi = k_A z$, where $k_s = \omega_{pe}/c$.

The expressions for the components of the scaled electric and magnetic fields (η_j, b_j) take the form

$$\eta_x = \frac{E_x}{\mathcal{A}_E} = \psi \int_0^\infty d\kappa\, \kappa \sqrt{1+\kappa^2} e^{-\kappa^2 l_\perp^2/2} \times\left[\cos^2\phi\left(J_0(\overline{\rho}\kappa) - \frac{2J_1(\overline{\rho}\kappa)}{\overline{\rho}\kappa}\right) + \frac{J_1(\overline{\rho}\kappa)}{\overline{\rho}\kappa}\right] \times[Z(\zeta_2) - Z(\zeta_1) + i2\sqrt{\pi}e^{-\zeta_1^2}] + \text{c.c.}, \tag{17}$$

$$\eta_y = \frac{E_y}{\mathcal{A}_E} = \psi \sin\phi\cos\phi \int_0^\infty d\kappa\, \kappa \sqrt{1+\kappa^2} e^{-\kappa^2 l_\perp^2/2} \times\left[J_0(\overline{\rho}\kappa) - \frac{2J_1(\overline{\rho}\kappa)}{\overline{\rho}\kappa}\right][Z(\zeta_2) - Z(\zeta_1) + i2\sqrt{\pi}e^{-\zeta_1^2}] + \text{c.c.}, \tag{18}$$

$$\eta_z = \frac{E_z}{\mathcal{A}_E} = \psi\left(\frac{ik_A}{k_s}\right)\cos\phi \int_0^\infty d\kappa\, \kappa^2 e^{-\kappa^2 l_\perp^2/2} J_1(\overline{\rho}\kappa) \times[Z(\zeta_2) + Z(\zeta_1) - i2\sqrt{\pi}e^{-\zeta_1^2}] + \text{c.c.}, \tag{19}$$

$$b_x = \frac{B_x}{\mathcal{A}_B} = -\psi \sin\phi\cos\phi \int_0^\infty d\kappa\, \kappa\, e^{-\kappa^2 l_\perp^2/2}\left[J_0(\overline{\rho}\kappa) - \frac{2J_1(\overline{\rho}\kappa)}{\overline{\rho}\kappa}\right][Z(\zeta_2) + Z(\zeta_1) - i2\sqrt{\pi}e^{-\zeta_1^2}] + \text{c.c.}, \tag{20}$$

$$b_y = \frac{B_y}{\mathcal{A}_B} = \psi \int_0^\infty d\kappa\, \kappa\, e^{-\kappa^2 l_\perp^2/2} \times\left[\cos^2\phi\left(J_0(\overline{\rho}\kappa) - \frac{2J_1(\overline{\rho}\kappa)}{\overline{\rho}\kappa}\right) + \frac{J_1(\overline{\rho}\kappa)}{\overline{\rho}\kappa}\right] \times[Z(\zeta_2) + Z(\zeta_1) - i2\sqrt{\pi}e^{-\zeta_1^2}] + \text{c.c.} \tag{21}$$

Since the compressional mode is neglected, as explained earlier

$$b_z = \frac{B_z}{\mathcal{A}_B} = 0. \tag{22}$$

In Eqs. (17)–(22)

$$\psi \equiv \exp\left(\frac{-\xi^2}{2l_\parallel^2} + i(\xi - \omega t)\right), \tag{23}$$

$$\mathcal{A}_E = \frac{1}{2\sqrt{2}}\left(\frac{\delta n}{n_0}\right) l_\parallel l_\perp^2 E_p, \tag{24}$$

and

$$\mathcal{A}_B = \left(\frac{k_A}{k_0}\right)\mathcal{A}_E. \tag{25}$$

The Z-functions correspond to the usual plasma dispersion function[13] whose arguments are

$$\zeta_1 = \frac{-l_\parallel}{\sqrt{2}}\left(\sqrt{1+\kappa^2} + 1 + \frac{i\xi}{l_\parallel^2}\right), \tag{26}$$

$$\zeta_2 = \frac{l_\parallel}{\sqrt{2}}\left(\sqrt{1+\kappa^2} - 1 - \frac{i\xi}{l_\parallel^2}\right). \tag{27}$$

It should be emphasized that the appearance of the Z-functions in this calculation is not a consequence of kinetic behavior. Rather, it reflects the resonant excitation of a Gaussian-like $\delta\tilde{n}$ as given by Eq. (1). Other functional forms would result in generalizations of the familiar Z-function.

III. GENERAL FEATURES

Before discussing the results obtained from the full numerical integration of Eqs. (17)–(22), it is useful to extract the approximate analytic behavior in certain limits. To simplify the expressions, we examine here the dependence of the scaled magnetic field along the direction of polarization $(\hat{\mathbf{x}})$ of the primary wave for the choice $k_s y = 0$. At this location only the y component is present, i.e., $\mathbf{b}(k_s x, k_s y = 0, \xi, t) = b_y(k_s x, \xi, t)\hat{\mathbf{y}}$.

Near the axis of the density perturbation, $\overline{\rho} \ll 1$, the contribution from the Bessel functions in the integrands of Eq. (21) can be expanded in a power series to obtain the leading behavior

$$b_y \rightarrow \psi[g_1 - (k_s x)^2 g_2] + \text{c.c.}, \tag{28}$$

where

$$g_1 = \frac{1}{2}\int_0^\infty d\kappa\, \kappa\, e^{-\kappa^2 l_\perp^2/2}[Z(\zeta_2) + Z(\zeta_1) - i2\sqrt{\pi}e^{-\zeta_1^2}], \tag{29}$$

and

$$g_2=\frac{3}{16}\int_0^\infty d\kappa\,\kappa^3\,e^{-\kappa^2 l_\perp^2/2}[Z(\zeta_2)+Z(\zeta_1)-i2\sqrt{\pi}e^{-\zeta_1^2}]. \tag{30}$$

This expression indicates that at the center of the density perturbation a finite component of **b** develops and its strength exhibits a parabolic decrease with increasing transverse distance. Of course, along the z direction b_y follows a Gaussian pattern, as contained in the factor ψ.

For radial positions well outside the density perturbation (but still along $k_s y=0$), i.e., $\bar{\rho}\gg 1$, the Bessel functions in Eq. (21) are expanded in their asymptotic limit to yield

$$b_y\rightarrow\frac{\psi g_3}{\bar{\rho}^2}+\text{c.c.}, \tag{31}$$

where the coefficient g_3 is given by

$$g_3=[Z(\zeta_2(\kappa=0))+Z(\zeta_1(\kappa=0))-i2\sqrt{\pi}e^{-\zeta_1^2(\kappa=0)}]. \tag{32}$$

This expression indicates a relatively rapid fall-off of the magnetic fluctuation excited outside the ambient field lines connecting to the density perturbation. This is in contrast to the ρ^{-1} dependence of the patterns radiated by single-disk exciters in laboratory studies. The single disk exciters essentially behave as axial current modulators (i.e., single wires). The strong cancellation of the self-consistent axial currents associated with the inherent transverse exciter in the present problem has closer similarity to the double-disk configuration recently developed by Leneman *et al.*[10]

The axial variation of the parallel electric field for $\xi\ll 1$ is given by,

$$\eta_z\rightarrow i\cos\phi\,\frac{k_A}{k_s}e^{-i\omega t}[g_4+i\xi g_5]+\text{c.c.}, \tag{33}$$

where

$$g_4=\int_0^\infty d\kappa\,\kappa^2\,J_1(\kappa\bar{\rho})\,e^{-\kappa^2 l_\perp^2/2}[Z(\zeta_2(\xi=0))+Z(\zeta_1(\xi=0))-i2\sqrt{\pi}e^{-\zeta_1^2(\xi=0)}], \tag{34}$$

and

$$g_5=\int_0^\infty d\kappa\,\kappa^2\,J_1(\kappa\bar{\rho})\,e^{-\kappa^2 l_\perp^2/2}\times\left\{\frac{2\sqrt{2}}{l_\parallel}+\sqrt{1+\kappa^2}[Z(\zeta_2(\xi=0))-Z(\zeta_1(\xi=0))+i2\sqrt{\pi}e^{-\zeta_1^2(\xi=0)}]\right\}. \tag{35}$$

Next, we examine the spatial patterns of the small-scale electric and magnetic fields excited by the beat source. The results are obtained by direct numerical integration of Eqs. (17)–(22) for various parameter values of relevance to scenarios that can result in effective wave–particle interactions.

Figure 2 displays the variation of the magnitude of the scaled magnetic field $|\mathbf{b}|$ along the x direction, i.e., the direction of polarization of the pump wave. The field shown in Fig. 2 is calculated at $k_s y=0$ and $\xi=3$ for a density perturbation with perpendicular and parallel scale lengths of $l_\perp=1.0$ and $l_\parallel=0.1$. This corresponds to an axial location well outside the density perturbation, but not yet in the asymptotic region of wave propagation. In the region $k_s x\ll 1$ the quantity $|\mathbf{b}|$ approaches a constant value and exhibits a parabolic decrease, as expected from the limiting expression given by Eq. (28). For $k_s x>6$, the decreasing value of $|\mathbf{b}|$ is well represented by the asymptotic expression given by Eq. (31) (dashed curve). For reference, the profile of the density perturbation (dotted curve) is also shown in Fig. 2.

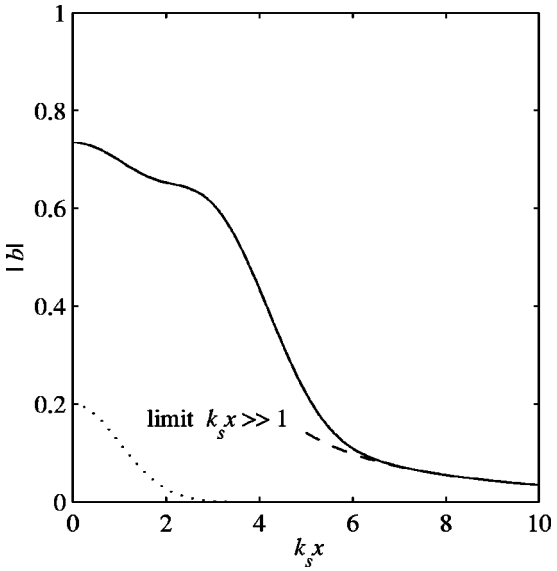

FIG. 2. Spatial variation of the magnitude of the scaled magnetic field along the direction of polarization of the pump wave at a position $k_s y=0$, $\xi=3$, and generated by a density perturbation (dotted curve) with $l_\perp=1$ and $l_\parallel=0.1$. Dashed line is the asymptotic result given by Eq. (31).

The axial dependence of the magnitude of the scaled parallel electric field $|\eta_z|$ is shown in Fig. 3 for a density perturbation with the same $l_\perp$ and $l_\parallel$ as in Fig. 2. The transverse position sampled corresponds to $k_s y=0$ and $k_s x=1.0$. $|\eta_z|$ exhibits a rapid increase within the source region ($k_s x<0.2$ where $\delta\tilde{n}$ is significant) and is well described by the limiting expression given by Eq. (33) (dashed curve). Again, for reference, the axial dependence of the density perturbation is shown by the dotted curve. Far from the source region, $|\eta_z|$ exhibits a slow decrease. The decrease results from the dispersive nature of shear Alfvén waves of small transverse scale (here due to finite electron inertia). Unfortunately, a useful asymptotic expression for $|\eta_z|$ is not readily available because its form is sensitive to the transverse position $(k_s x, k_s y)$ and thus requires numerical evaluation.

The arrow shown at the bottom of Fig. 3 indicates the axial location ($\xi=1$) of the two-dimensional structure of the transverse electric field vector displayed in Fig. 4. This pattern is generated by the same density perturbation considered in Figs. 2 and 3. The dotted circle in Fig. 4 indicates the contour where $\delta\tilde{n}$ achieves one-half of its peak value. It is evident from Fig. 4 that the transverse component of the

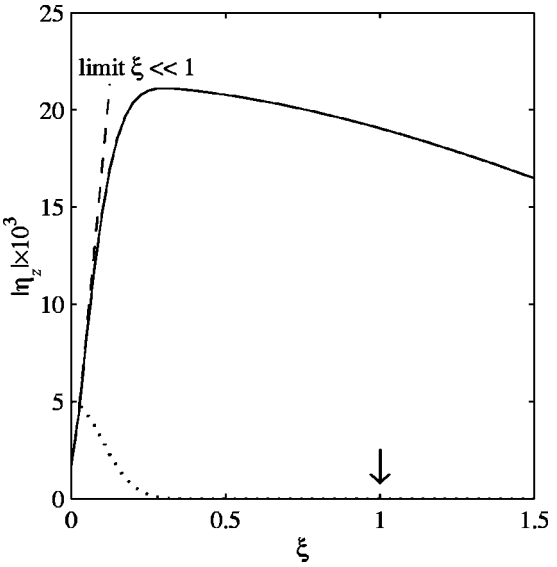

FIG. 3. Axial dependence of the magnitude of the scaled parallel electric field in the region $z>0$, at a transverse position $k_s x=1$, $k_s y=0$, for a density perturbation with the same $l_\perp$ and $l_\parallel$ as in Fig. 2. Dotted curve is the density perturbation and $\xi=k_A z$. Dashed curve is the approximate behavior predicted by Eq. (33). Arrow indicates axial position of transverse field patterns shown in Figs. 4 and 5.

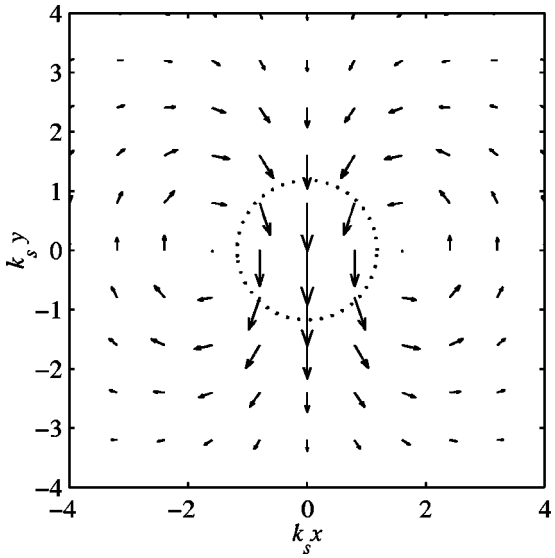

FIG. 5. Two-dimensional structure of the magnetic field vector at the axial position ($\xi=1$) indicated by the arrow in Fig. 3. The dotted circle corresponds to the contour where $\delta\tilde{n}$ is one-half its peak value. Parameters of density perturbation are the same as in Figs. 2–4.

electric field is predominantly electrostatic (an approximation often made in descriptions of shear Alfvén waves) and its source can be traced primarily to two charge concentrations centered at locations where $\nabla_\perp \cdot \mathbf{j}_s$ is maximum (along the symmetry line $k_s y=0$).

Figure 5 displays the two-dimensional pattern of the self-consistent magnetic field vector associated with the electric field pattern shown in Fig. 4. Again, the dotted circle corresponds to where $\delta\tilde{n}$ achieves one-half of its peak value. The magnetic field exhibits a pattern characteristic of a source consisting of parallel wires carrying equal and opposite currents, thus elucidating the reason behind the ρ^{-2} decrease given by Eq. (31). Physically, the equivalent parallel wires correspond to the parallel electron currents required to provide the cancellation of the two charge concentrations in the transverse direction identified in Fig. 4, and which are a consequence of gradients in the ion polarization currents.

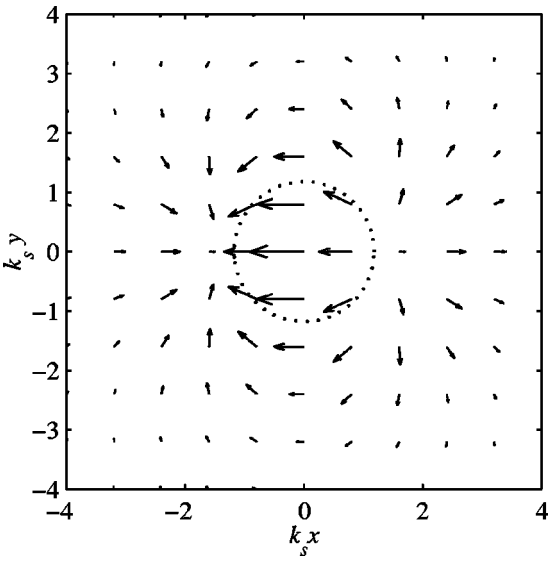

FIG. 4. Two-dimensional structure of the transverse electric field vector at the axial position ($\xi=1$) indicated by the arrow in Fig. 3. The dotted circle corresponds to the contour where $\delta\tilde{n}$ is one-half of its peak value. Parameters of density perturbation are the same as in Figs. 2 and 3.

An important feature of shear Alfvén waves of small transverse scale in low-β plasmas ($\beta_e \ll m/M$) is that they exhibit a spreading across the confining magnetic field which is bounded by an asymptotic angle (or cone angle) given by $\tan\theta_c=(\omega/\Omega_i)\sqrt{m/M}$. In the present problem, the *in situ* antenna is continuously distributed. Thus, it does not exhibit the sharp cones inherent in antennas used in laboratory studies. The spreading of the small-scale wave radiated by the density perturbation is determined by the superposition of a continuous distribution of cone angles whose origin varies according to the spatial form of $\delta\tilde{n}$. Figure 6 displays the spreading in the x direction exhibited by the magnitude of the scaled magnetic field $|\mathbf{b}|$ at a location $k_s y=0$ (line of symmetry) for different axial positions and for the same density perturbation leading to Figs. 2–5. The pairs of vertical bars near the top of Fig. 6 correspond to the predicted x position of the asymptotic cones that emanate from the center of the source ($k_s x=0$) and from a point at the location where $\delta\tilde{n}$ achieves half of its maximum value. For reference, the spatial form of $\delta\tilde{n}$ is indicated by the dotted curve. The region where $|\mathbf{b}|$ achieves significant values is consistently bounded (in the x direction) by the locations corresponding to the characteristic cone angles. At large values of $k_s x$, outside the cone trajectories, the patterns for the different axial positions approach the asymptotic behavior predicted by Eq. (31). Physically, this implies that the two axial current channels (of opposite polarity) spread out gradually due to the collisionless skin-depth effect, but remain confined within the region bounded by the cone trajectories.

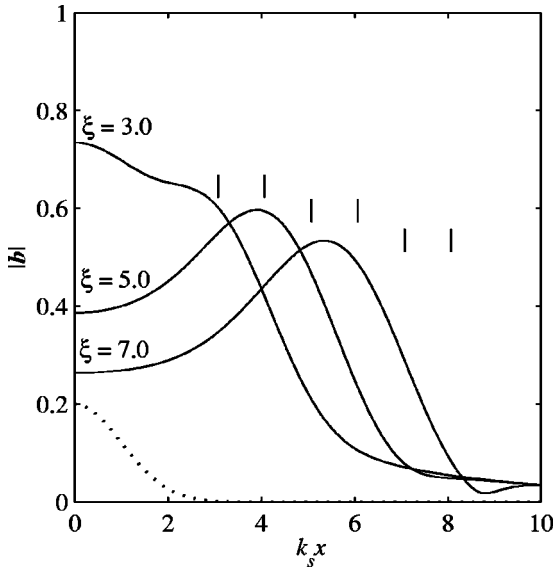

FIG. 6. Dependence of the magnitude of the scaled magnetic field at $k_s y = 0$ (line of symmetry) for different axial positions $\xi = k_A z$. The pairs of vertical bars correspond to the x position of asympotic cones (explained in the text). The spatial form of $\delta\tilde{n}$ is indicated by the dotted curve; $l_\parallel$ and $l_\perp$ as in Figs. 2–5.

The axial dependence of the magnitude and of the real part of the parallel electric field at $k_s x = 1$ and $k_s y = 0$ are shown in Fig. 7. A rapid rise in $|\eta_z|$ occurs at the center of the source ($\xi = 0$), while outside the density perturbation a wave with increasing wavelength develops along the positive and negative z directions. The reason for the near symmetry of the patterns along the positive and negative z directions in Fig. 7 is that they correspond to the condition $l_\parallel = 0.1$. In this limit, the pump wave essentially resembles, locally, the electric field generated by a large capacitor plate. Hence, the effective *in situ* antenna is nearly symmetric.

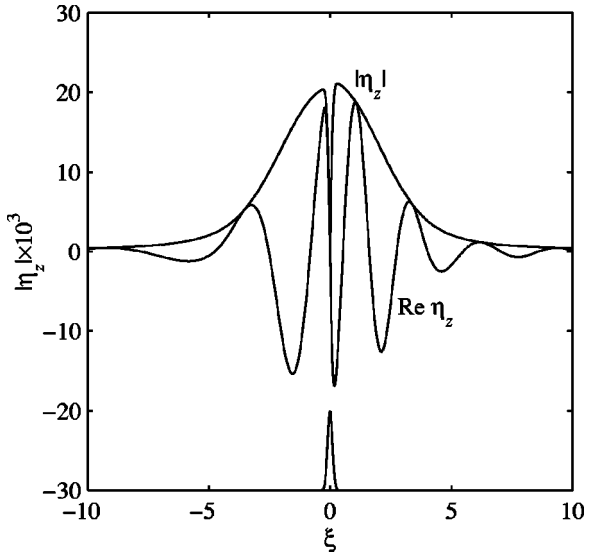

FIG. 7. Axial dependence of the real part and of the magnitude of the scaled parallel electric field for $k_s x = 1$, $k_s y = 0$. The solid bump at the bottom corresponds to $\delta\tilde{n}$; $l_\perp$ and $l_\parallel$ as in Figs. 2–6. $\xi = k_A z$.

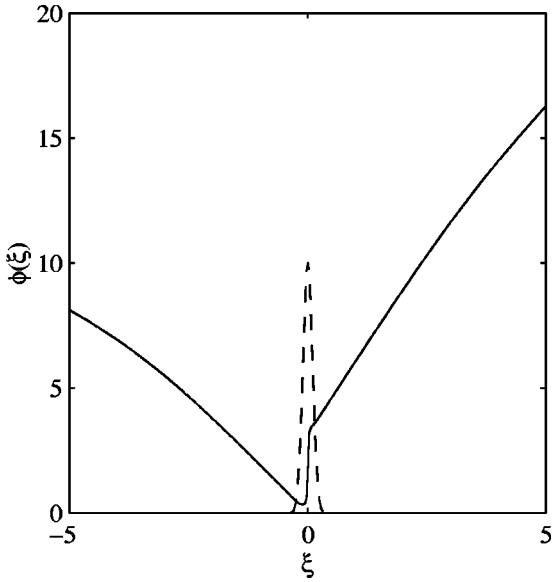

FIG. 8. Axial dependence of the phase of the parallel electric field of Fig. 7 shows that right and left-going waves are excited. Dashed curve is $\delta\tilde{n}$. $\xi = k_A z$.

Figure 8 illustrates the axial behavior of the phase of the parallel electric field pattern associated with Fig. 7. Figure 8 indicates that the signal propagating to the right (moving in the same direction as the pump wave) undergoes a rapid phase jump across the *in situ* antenna, indicated by the dotted curve. The local phase velocity associated with the phase variation of Fig. 8 is shown in Fig. 9. It is seen that the phase velocity of the wave propagating along the **k** of the pump wave experiences a significant decrease at axial positions well outside the density perturbation, while the wave propagating opposite the **k** of the pump wave approaches the asymptotic value, v_A, more rapidly.

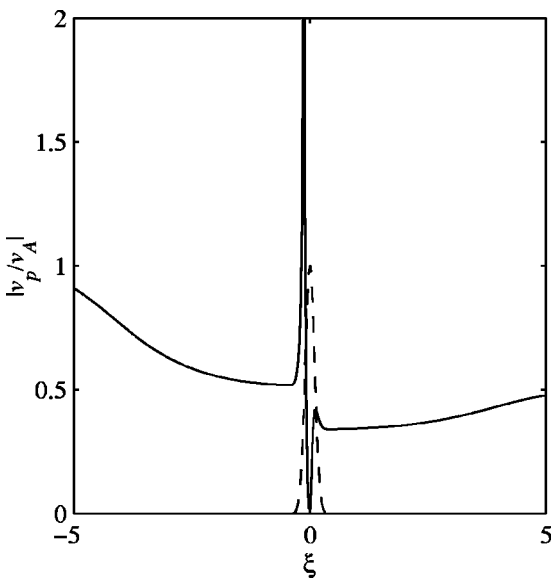

FIG. 9. Local phase velocity (scaled to Alfvén speed) associated with the axial phase variation of Fig. 8. Dashed curve is $\delta\tilde{n}$. $\xi = k_A z$.

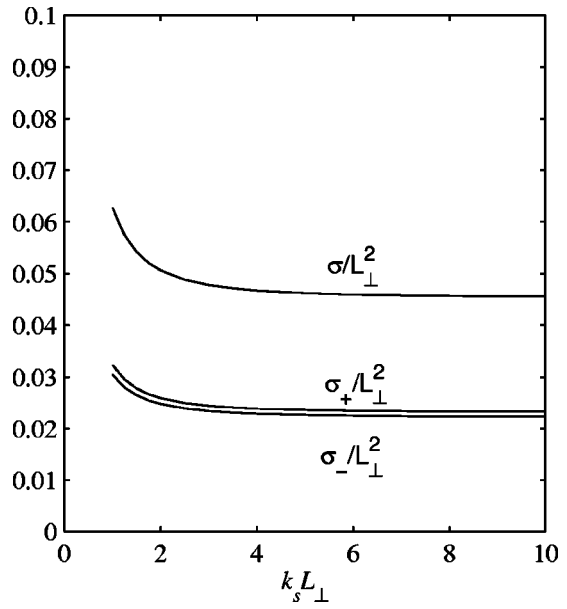

FIG. 10. Dependence of the scattering cross sections on the transverse scale of the density perturbation for a fixed parallel scale $l_\parallel = k_A L_\parallel = 0.1$. k_s^{-1} is the electron skin-depth and k_A is the Alfvén wave number of the pump wave.

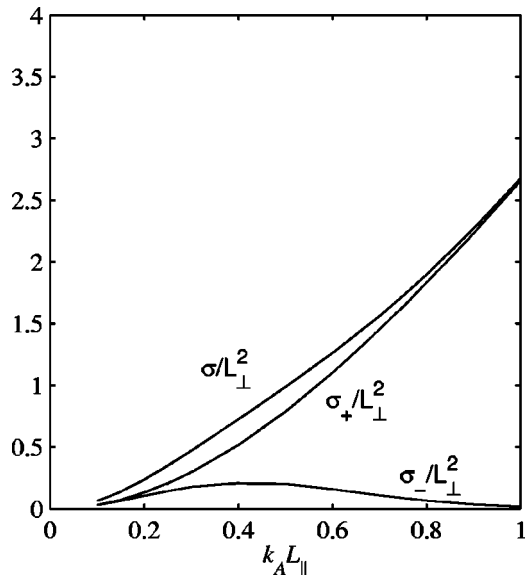

FIG. 11. Dependence of the scattering cross sections on the parallel scale of the density perturbation for a fixed transverse scale $l_\perp = k_s L_\perp = 1$. k_s^{-1} is the electron skin-depth and k_A is the Alfvén wave number of the pump wave.

IV. CROSS SECTION

Since in this study we envision the density perturbation to have spatial scales that are small compared to those of the pump wave, it is useful to summarize the energetic aspects of the interaction in terms of an effective scattering cross-section σ. Furthermore, since the modes radiated by the *in situ* antenna are highly collimated in the forward and backward z directions (within the small cone angle) the two dominant contributions can be individually associated with cross sections along and opposite $\mathbf{k}$ of the pump wave, σ_+ and σ_-, respectively.

The useful definitions of these quantities are

$$\sigma = \sigma_+ + \sigma_- , \tag{36}$$

with

$$\sigma_\pm = \int_{-\infty}^{\infty} k_s\, dy \int_{-\infty}^{\infty} k_s dx \, \frac{\langle S_z^\pm (k_s x, k_s y, \xi \to \pm\infty)\rangle}{\langle S_0\rangle (\delta n/n_0)^2}, \tag{37}$$

where S_z is the power flux associated with the small-scale waves radiated, i.e., $S_z^\pm = \pm \mathbf{S}\cdot\hat{\mathbf{z}}$ with $\mathbf{S} = (c/4\pi)\mathbf{E}\times\mathbf{B}$ the self-consistent Poynting vector of the small-scale waves. The angular brackets correspond to the usual time average and S_0 is the z component of the Poynting vector of the pump wave. The definition given in Eq. (37) also normalizes out the contribution from the peak amplitude of the density fluctuation, i.e., the term $(\delta n/n_0)^2$. Furthermore, since the $\sigma_\pm$ represent an effective area in the transverse direction, in discussing their properties it is useful to scale them to the effective geometrical area $(L_\perp^2)$ associated with the density perturbation.

The dependence of the scattering cross sections on the transverse scale of the density perturbation is shown in Fig. 10 for a parallel scale length $l_\parallel = 0.1$. For $l_\perp > 3$ the efficiency of the transformation to small scales saturates and rises steeply as $l_\perp \to 1$. Within the present model, σ would continue to increase for smaller $l_\perp$, but physically other effects (e.g., finite ion Larmor radius) would limit such a behavior. It is also seen from Fig. 10 that σ_+ and σ_- are nearly equal, which again, is a consequence of the near symmetry of the source that results for small values of $l_\parallel$.

The corresponding dependence of the cross sections on the parallel scale length of the density perturbation is shown in Fig. 11 for a transverse scale length $l_\perp = 1$. It is found that a significant departure between forward and backward scattering develops for $l_\parallel > 0.3$. The forward cross section increases monotonically while the backward cross section decreases rapidly. Both of these behaviors can be recovered by approximate analytical expressions derived from Eq. (37), but the relevant manipulations are lengthy and are not worth reproducing here. Physically, the reason for the increase in the forward cross section is that the length of the *in situ* antenna is increasing and hence approaches optimal tuning. At the same time, the backward radiation suffers a corresponding detuning because the phase of source current advances in the opposite direction. The increase in σ_+ as $l_\parallel$ increases would eventually saturate because when $l_\parallel$ becomes comparable to the axial wavelength of the pump wave a cancellation results from the opposite phases sampled. From the motivations of the present calculation, however, we do not envision that $l_\parallel$ would achieve such large values.

V. CONCLUSION

The present analytic study has examined the detailed properties of the interaction between a shear Alfvén wave propagating along the confining magnetic field in a low-β plasma and a pre-existing density perturbation having small transverse scale. The polarization velocity, induced by the primary (or pump) wave on the plasma ions, beats with the

density perturbation to produce an extended in-situ source having an azimuthal dependence about the confining magnetic field. This effective antenna radiates forward and backward shear waves of small transverse scale that develop parallel electric fields. When suitable conditions are attained, these parallel fields can result in parallel electron acceleration.

This study has found that the *in-situ* antenna gives rise to two self-consistent, field-aligned current filaments of opposite polarity. The asymptotic magnetic field associated with these current filaments decays radially as ρ^{-2}. As the dipolar current filaments propagate away from the source they exhibit a radial spreading that is bounded by the cone trajectories associated with inertial Alfvén waves of small-transverse scale.

The combined structure formed by the radiated electric and magnetic fields exhibits a complexity suggestive of nonlinear vortices. However, it must be emphasized that the underlying physics behind such structures is entirely due to linear processes. This perspective is important when interpreting measurements taken in the laboratory and on board spacecraft. In particular, one can envision the results of several wave transformation events that, when viewed from locations far from their origin, would appear to be due to some form of turbulence.

A useful expression has been found that allows the assessment of the magnitude of the parallel electric fields that can arise from interactions with density perturbations. From the scaling quantity $\mathcal{A}_E$ given by Eq. (24) and the numerical result shown in Fig. 7 it follows that $\max|\eta_z| \sim 10^{-2}(\delta n/n_0) l_\parallel l_\perp^2 E_p$ which for the expected characteristic conditions of $l_\perp \sim 1$ would result in a parallel energy gain of $\Delta U_\parallel \sim 10^{-3}(\delta n/n_0)(eE_p L_\parallel)$, which explicity exhibits the elements of efficiency of the transformation process. In here, e is the quantum of charge and E_p is the magnitude of the transverse electric field of the large-scale wave.

It has been identified that the energetics of the scale transformation process considered can be succinctly summarized by an effective scattering cross section. The cross section approaches a constant value for large transverse scales and rises sharply as the condition $l_\perp \lesssim 1$ is attained. As the parallel scale of the density perturbation increases the forward cross section increases while the backward decreases. For $l_\parallel < 0.2$ the efficiency of radiation in the forward and backward directions is nearly identical. From the scaling of the cross section inherent in the definition of Eq. (37) and the result of Fig. 11 one finds that the fractional power extracted from the large scale mode by the density perturbation is approximately equal to $(\delta n/n_0)^2$.

In summary, this work elucidates a mechanism for the transformation of the energy stored in large scales in environments in which a sizeable level of density fluctuations are present.

ACKNOWLEDGMENTS

This work is sponsored by the Office of Naval Research and the U.S. Department of Energy.

[1] J. F. Drake, R. G. Kleva, and M. E. Mandt, Phys. Rev. Lett. **73**, 1251 (1994).
[2] A. Strelsov and W. Lotko, J. Geophys. Res. **100**, 19,457 (1995).
[3] U. Narain and P. Ulmschneider, Space Sci. Rev. **54**, 377 (1990).
[4] T. Ohkawa, Phys. Lett. A **67**, 35 (1978).
[5] G. J. Morales, S. N. Antani, and B. D. Fried, Phys. Fluids **28**, 3302 (1985).
[6] J. F. Bamber, J. E. Maggs, and W. Gekelman, J. Geophys. Res. **100**, 23,795 (1995).
[7] T. F. Bell, H. G. James, U. S. Inan, and J. P. Katsufrakis, J. Geophys. Res. **88**, 4813 (1983).
[8] A. Y. Wong, G. J. Morales, D. Eggleston, J. Santoru, and R. Behnke, Phys. Rev. Lett. **47**, 1340 (1981).
[9] W. Gekelman, D. Leneman, J. Maggs, and S. Vincena, Phys. Plasmas **1**, 3775 (1994).
[10] D. Leneman, W. Gekelman, and J. Maggs, Phys. Rev. Lett. **82**, 2673 (1999).
[11] G. J. Morales, R. S. Loritsch, and J. E. Maggs, Phys. Plasmas **1**, 3765 (1994).
[12] G. J. Morales and J. E. Maggs, Phys. Plasmas **4**, 4118 (1997).
[13] B. D. Fried and S. D. Conte, *The Plasma Dispersion Function: The Hilbert Transform of the Gaussian* (Academic, New York, 1961).